

Investigating Data Hierarchies in Multifidelity Machine Learning for Excitation Energies

Vivin Vinod¹[0000-0001-6218-5053] and Peter Zaspel¹[0000-0002-7028-6580]

School of Mathematics and Natural Science, University of Wuppertal, Wuppertal 42119, Germany
{vinod,zaspel}@uni-wuppertal.de

Abstract. Recent progress in machine learning (ML) has made high-accuracy quantum chemistry (QC) calculations more accessible. Of particular interest are multifidelity machine learning (MFML) methods where training data from differing accuracies or fidelities are used. These methods usually employ a fixed scaling factor, γ , to relate the number of training samples across different fidelities, which reflects the cost and assumed sparsity of the data. This study investigates the impact of modifying γ on model efficiency and accuracy for the prediction of vertical excitation energies using the QeMFi benchmark dataset. Further, this work introduces QC compute time informed scaling factors, denoted as θ , that vary based on QC compute times at different fidelities. A novel error metric, error contours of MFML, is proposed to provide a comprehensive view of model error contributions from each fidelity. The results indicate that high model accuracy can be achieved with just 2 training samples at the target fidelity when a larger number of samples from lower fidelities are used. This is further illustrated through a novel concept, the T -curve, which compares model error against the time-cost of generating training samples, demonstrating that multifidelity models can achieve high accuracy while minimizing training data costs.

Keywords: multifidelity · machine learning · quantum chemistry · DFT · excitation energies · sparse data

1 Introduction

Machine learning (ML) and quantum chemistry (QC) have become increasingly interlinked over the recent times. Both have seen rapid development in tandem allowing for quick prediction of QC properties in place of the costly conventional calculations [1, 2, 9, 10, 15, 23]. This has allowed researchers to perform preliminary examination of complex QC problems with much speed. The ML-QC pipeline first identifies a QC property of interest. Next, a training set is calculated for a desired QC method, say Density Functional Theory (DFT); this is also referred to as a *fidelity*, that is, the level of accuracy of the method with respect to what would be considered ground truth. Once a training dataset is computed, a ML model of choice is trained.

The bottleneck in such a pipeline is often the high cost of generating training data. A ML model can only be as good as the data it is trained on. It is often noted that a larger number of training samples results in a more accurate ML model [4, 23]. This observation implies that either one needs to use a less accurate, and thereby less expensive QC method to train the ML model, or have less training samples at a higher fidelity thereby, resulting in a less accurate ML model, when it comes to the prediction error relative to the data. Several methodological improvements over the single fidelity ML methods for QC have been proposed to overcome this hurdle in the ML-QC pipeline, including Δ -ML [12], where one trains on the difference between two fidelities. This method has been shown to

reduce the number of training samples needed at the expensive fidelity and has since been modified in various flavors including hierarchical ML [5], multifidelity ML (MFML) [11, 18, 24], and optimized MFML (o-MFML) [17]. MFML and its variant of o-MFML, systematically combine several Δ -ML like models with more than two fidelities. This method has been shown to be superior in predicting excitation energies along molecular trajectories [18]. A recent work has also introduced the use of multitask Gaussian processes to harness heterogeneous multifidelity data in order to predict three-body interaction energy in water trimer with coupled cluster accuracy [6]. MFML differs from the conventional Δ -ML method not just in terms of the number of fidelities that are used but also in the number of training samples used at each fidelity. Conventionally, the Δ -ML method uses the same number of samples at both the fidelities. In MFML, these training samples are scaled down as one increases the fidelity of the training data. This further reduced the number of costly training samples needed at the highest fidelity, also called the *target fidelity*. This *scaling factor*, in previous studies was set to be 2, meaning that at each subsequently lower fidelity, the number of training samples would be scaled up by a factor of 2 [17–19, 24]. Ref. [24] discusses that the scaling factor of 2 for MFML was decided based on previous work related to sparse grid combination methods [7, 8, 13].

This work assesses scaling factors that are different from those used thus far in literature. Several fixed scaling factors, that is, the same scaling factors across the different fidelities are tested. These are evaluated on the recently released benchmarking multifidelity dataset, QeMFi [20, 21], which consists of 135,000 geometries of nine complex molecules. Since the QeMFi dataset also provides the compute time for each fidelity for each molecule type, two time-cost informed scaling factors are also assessed.

The *scaling factor*, the ratio of training samples used at two consecutive fidelities, or levels, directly controls the total number of training samples used for MFML and thereby the cost of generating a training set for the approach. Understanding the effect of this parameter in the efficiency and accuracy of the MFML approach would potentially provide opportunities to further improve the overall multifidelity approach for QC. Studying model accuracy in relation to the cost of generating the training set for the model also provides a robust measure of how the diverse MFML models behave with respect to the single fidelity models as has been shown in refs. [18, 20]. Therefore, assessment of model accuracy and time-cost of generating corresponding training data is made for the diverse scaling factors. In interest of a complete investigation not only into the scaling factors but also into better understanding the multifidelity data structure, this work further introduces a new error metric for multifidelity methods for QC, namely *error contours* of MFML. Error contours describe the model error with respect to training samples used at two fidelities thereby giving a more comprehensive analysis of the contribution of each fidelity to the overall accuracy of the MFML model. The study of the error contours of MFML indicates that using much lower training samples at the costlier fidelity while increasing the number of training samples at the lowest fidelity results in an MFML model of high accuracy at a much lower cost than the conventional MFML approach with a fixed scaling factor. To systematically assess this, this work studies multifidelity models built with a small number of fixed training samples at the target fidelity and increasing the scaling factor. This gives rise to the notion of the Γ -curve as delineated in section 2.6. The models that are built in such a manner are shown to be superior to the conventional MFML approach in terms of model error for a given cost of generating the training data.

The rest of this manuscript is structured as follows: all the methodological pre-requisites including dataset details are presented in section 2. The concepts of scaling factors and the tools used in this work are also explained in detail. This is followed by the results of MFML and o-MFML models for the prediction of excitation energies with the different scaling factors in section 3. In

addition to the time-cost of the different MFML models in section 3.2, the error contours of MFML and the Γ -curves are studied in sections 3.3 and 3.4 respectively. Inferences on these results are made followed by a discussion and outlook of this work along with its implications for future work in multifidelity methods.

2 Methods

This section discussed the various methodological pre-requisites needed to appreciate the results and inferences of this work. First, the dataset used is introduced and the multifidelity structure explained. This is followed by the ML details including KRR, MFML, and o-MFML. The section also discusses the concept of scaling factors in detail, to establish the conceptual motivation behind this work.

2.1 Dataset

The QeMFi dataset [20, 21] is a recently released benchmark dataset of diverse molecules of varying chemical conformations. These molecules include urea, 2-nitrophenol, and thymine among others. It contains a total of 135,000 point geometries with diverse QC properties such as the first 10 vertical excitation energies in addition to the compute time for each molecule for each fidelity. These properties are calculated with the DFT formalism with five different basis sets, which in turn form the ordered multifidelity hierarchy. In increasing order of accuracy, these are STO3G, 321G, 631G, def2SVP, and def2TZVP. In this work, these fidelities are hereon referred to only with the basis set names, and often with the shortened notation such as TZVP for def2TZVP.

The first excitation energies were taken from QeMFi as the property to be studied with the different data scaling applied. While QeMFi provides various other QC properties such as ground state energies and molecular dipole moments, the excitation energies are chosen since they are generally more challenging for ML model [3, 23] than ground state energies. Although there is increasing interest in vector properties such as molecular dipole moments, these are not studied here since they would require an extensive discussion of equivariance and invariance of molecular descriptors [16, 22], that is the map between the Cartesian coordinates and machine learnable input features. This discussion lies out of the scope of this current work. Thus the excitation energies of QeMFi are used herein. The energies are reported in cm^{-1} . As a first step, from the 135,000 total geometries in QeMFi, 120,000 were randomly sampled to form the diverse training sets. From the remaining 15,000 geometries, a validation set of 2,000 samples was set aside to be used in the o-MFML method. Finally, the remaining 13,000 samples were set aside as a test set. Both the validation set and the test set are not changed over the course of this entire study, that is, all errors are reported on the same test set. It is to be noted that the test set is never used during the training or validation phases of any of the models. Therefore the error reported by the models is on a set of truly unseen data. The validation set and the test set are fixed and not changed during the course of the experiments in this work.

In order to assess the efficiency of the multifidelity models vis-à-vis the single fidelity model, the time-cost of generating the training data versus model error are studied. For this purpose, the QC-compute time of each fidelity is considered from the QeMFi dataset. As ref. [20] notes, the QC-compute time provided in the dataset is the time of a single-core QC-calculation of a fidelity for a given molecule. To compute the training dataset generation time, these calculation times are used.

2.2 Kernel Ridge Regression

Given a fidelity, f , consider a training set of molecular representations and corresponding excitation energies given by $\mathcal{T}^{(f)} := \{(\mathbf{X}_i, y_i^{(f)})\}_{i=1}^{N_{\text{train}}}$. The molecular representations used in this assessment are the unsorted Coulomb Matrix(CM) [14] representations. For a given molecule, these are calculated as

$$C_{i,j} := \begin{cases} \frac{Z_i^{2.4}}{2}, & i = j \\ \frac{Z_i \cdot Z_j}{\|\mathbf{R}_i - \mathbf{R}_j\|}, & i \neq j, \end{cases} \quad (1)$$

where, Z_i is the atomic charge for the i^{th} atom and its Cartesian coordinates are given by \mathbf{R}_i . The resulting representation for a molecule is then flattened into a 1-D array. Since the CM representation is symmetric for the atomic indices, a molecule with m atoms is therefore represented by a 1-D array of size $m(m-1)/2$. The QeMFi dataset consists of molecules of differing number of atoms, therefore the CM are padded with zero to match with the size of the CM representation of the largest molecule of the dataset which is o-HBDI with 23 atoms. This corresponds to a padded representation size of 253 entries per geometry.

For a query CM representation given as \mathbf{X}_q , the prediction of energies at fidelity f are given by:

$$P_{\text{KRR}}^{(f)}(\mathbf{X}_q) := \sum_{i=1}^{N_{\text{train}}^{(f)}} \alpha_i^{(f)} k(\mathbf{X}_q, \mathbf{X}_i), \quad (2)$$

where, $k(\cdot, \cdot)$ is the kernel function. In this work, the Matérn kernel of first order and discrete L_2 norm is used across the KRR models built. The Matérn kernel for two CM representations is computed as

$$k(\mathbf{X}_i, \mathbf{X}_j) = \exp\left(-\frac{\sqrt{3}}{\sigma} \|\mathbf{X}_i - \mathbf{X}_j\|_2\right) \cdot \left(1 + \frac{\sqrt{3}}{\sigma} \|\mathbf{X}_i - \mathbf{X}_j\|_2\right), \quad (3)$$

where, σ is the kernel length-scale parameter. The coefficients of KRR, $\boldsymbol{\alpha}^{(f)}$ from Eq. (2), are computed by solving $(\mathbf{K} + \lambda \mathbf{I})\boldsymbol{\alpha}^{(f)} = \mathbf{y}^{(f)}$ with \mathbf{K} called the kernel matrix whose entries are simply the result of the kernel function from Eq. (3) for each molecule pair in the training set. In Eq. 2, λ is a parameter that penalizes overfitting.

2.3 Multifidelity Machine Learning

Refs. [17, 24] have shown that the multifidelity machine learning (MFML) model for some QC property can be built by systematically combining individual *sub-models* that are themselves trained for a given fidelity, f . Within this approach, each sub-model is then identified by the fidelity and the corresponding number of training samples used, $N_{\text{train}}^{(f)}$. This is carried out by a composite index, $\mathbf{s} = (f, \eta_f)$, where $2^{\eta_f} = N_{\text{train}}^{(f)}$.

In mathematical formalism, a MFML model is given as:

$$P_{\text{MFML}}^{(F, \eta_F; f_b)}(\mathbf{X}_q) := \sum_{\mathbf{s} \in \mathcal{S}^{(F, \eta_F; f_b)}} \beta_{\mathbf{s}} P_{\text{KRR}}^{(\mathbf{s})}(\mathbf{X}_q), \quad (4)$$

where, the linear combination is performed over the set of selected sub-models of MFML, $\mathcal{S}^{(F, \eta_F; f_b)}$. This selection is decided by the choice of the *baseline fidelity*, f_b , and the number of training samples

at the highest fidelity (also called the target fidelity), $N_{\text{train}}^{(F)} = \eta_F$. The sub-models for a MFML model with a given F , η_F , and f_b are identified as discussed previously in ref. [17]. In Eq. (4), $\beta_{\mathbf{s}}$ are the coefficients of the linear combination of these selected sub-models.

For MFML, the $\beta_{\mathbf{s}}$ are selected as

$$\beta_{\mathbf{s}}^{\text{MFML}} = \begin{cases} +1, & \text{if } f + \eta_f = F + \eta_F \\ -1, & \text{otherwise} \end{cases}, \quad (5)$$

based on ref. [24].

Recently, a methodological development over conventional MFML was proposed and shown to be superior to MFML in ref. [17]. Termed optimized MFML (o-MFML), it optimizes the combination of the sub-models of MFML. In other words, it considers coefficient values different from those defined in Eq. (5) for the different sub-models by optimizing over a validation set $\mathcal{V}_{\text{val}}^F := \{(\mathbf{X}_q^{\text{val}}, y_q^{\text{val}})\}_{q=1}^{N_{\text{val}}}$. With some target fidelity, F with η_F given and a baseline fidelity f_b chosen, one can formally define the o-MFML model as:

$$P_{\text{o-MFML}}^{(F, \eta_F; f_b)}(\mathbf{X}_q) := \sum_{\mathbf{s} \in \mathcal{S}^{(F, \eta_F; f_b)}} \beta_{\mathbf{s}}^{\text{opt}} P_{\text{KRR}}^{(\mathbf{s})}(\mathbf{X}_q), \quad (6)$$

where $\beta_{\mathbf{s}}^{\text{opt}}$ are the optimized coefficients of MFML. These values are attained by solving the optimization problem

$$\beta_{\mathbf{s}}^{\text{opt}} = \arg \min_{\beta_{\mathbf{s}}} \left\| \sum_{v=1}^{N_{\text{val}}} \left(y_v^{\text{val}} - \sum_{\mathbf{s} \in \mathcal{S}^{(F, \eta_F; f_b)}} \beta_{\mathbf{s}} P_{\text{KRR}}^{(\mathbf{s})}(\mathbf{X}_v^{\text{val}}) \right) \right\|_p, \quad (7)$$

where one minimizes some p -norm on the validation set defined above. The optimization procedure used in this work is ordinary least squares (OLS) which uses a $p = 2$ norm.

2.4 Scaling Factors

Thus far, in both MFML and o-MFML, the number of training samples used for each fidelity are scaled by a *scaling factor* of $\gamma = 2$ based on research on sparse grid combination methods [7, 8, 13]. For example, if one has $N_{\text{train}}^{(F)} = 32$ training samples for fidelity F then it is that $N_{\text{train}}^{(F-1)} = 64$ training samples for fidelity $F - 1$, $N_{\text{train}}^{(F-2)} = 128$ training samples on fidelity $F - 2$, and so on. The scaling up of the training samples as one decreases the fidelities can be thought of intuitively from a perspective of sparseness of data. As one increases the fidelity, the cost of QC calculation increases. This results in lower number of point-calculations that need to be made at this fidelity.

The scaling factor can itself be varied to assess its effect on the model error. This work tests five such scaling factors, in particular, $\gamma \in \{2, 3, 4, 5, 6\}$. For each of these scaling factors, the training set size increases exponentially as one goes down the fidelities. If one starts with N_{train}^F samples at the target fidelity, then at each lower fidelity, $f < F$, the number of training samples would be $N_{\text{train}}^f = \gamma^{F-f} \times N_{\text{train}}^F$. As an example, if $F = 5$, $N_{\text{train}}^F = 2$, and $\gamma = 3$, then for $f_b = 1$ the training set size for each fidelity, in increasing order of the fidelity, would be $\{3^4 \cdot 2, 3^3 \cdot 2, 3^2 \cdot 2, 3 \cdot 2, 2\}$.

This work studies two additional approaches for QC-cost adapted selection of scaling factors. This approach takes into account the compute times for each fidelity before adaptively selecting the ratio of training samples between two consecutive fidelities. The QeMFi dataset provides the

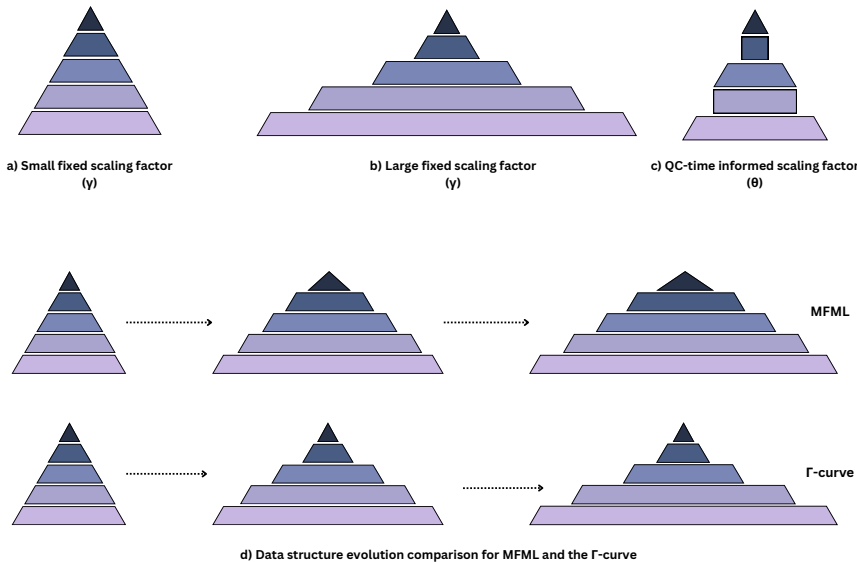


Fig. 1: A hypothetical comparison of training data used across fidelities for the different kinds of scaling factors used in this work. a) The multifidelity training data structure used in MFML with a small fixed scaling factor (γ). b) Multifidelity training data structure for a large fixed scaling factor (γ) results in a larger number of training samples being used at the cheaper fidelities. c) The structure of multifidelity training data used for scaling factors that are decided based on the QC-time cost, explained in section 2.4 as θ_f^f and θ_{f-1}^f . d) Comparison of training data structure evolution for conventional MFML and the Γ -curve introduced in section 2.6. Notice how the number of training samples used at the target (the costliest) fidelity remain same across the data structure for the Γ -curve while they increase for the conventional MFML method.

QC compute time in seconds for each of the five fidelities when computed on a single core. This information can be used to determine a time-informed scaling factor for each fidelity as opposed to setting a single scaling factor for all the fidelities. While there could be different ways to determine these scaling factors, the most trivial approach is to take the nearest integer value of the ratio of the compute times for the subsequent fidelity. That is, one can define $\theta_{f-1}^f := \lfloor T^f / T^{f-1} \rfloor$, where $\lfloor \cdot \rfloor$ denotes integer rounding. This specific choice of scaling factors is made to take into account the relative time-cost of the fidelities used in the MFML model. It is reasonable to assume that the number of training samples used at consecutive fidelities should be based on the ratio of the cost of those fidelities. Since QeMFi is a collection of different molecules, this approach was carried out with reference to the compute times for the largest molecule in the database: o-HBDI. This results in scaling factors $\theta_{f-1}^f = \{3, 1, 2, 1\}$ for increasing fidelity. That is, at SVP, the same number of training samples as TZVP are used while at the 631-G fidelity, it is twice, and so on. However, MFML models are built in such a way that subsequently cheaper fidelities have some more training samples than the previous fidelity so that the difference between the sub-models can be taken. In order to achieve this, after the number of training samples are decided by the scaling factors, if

fidelity $f - 1$ has the same number of training samples as fidelity f , then one additional sample is added to the sub-model at fidelity $f - 1$. As an example, if $N_{train}^{TZVP} = 2$, then the training samples for the different fidelities would be $\{12, 4 + 1, 4, 2 + 1, 2\}$. Hereon, the MFML models built with this approach of scaling factors are referred by θ_{f-1}^f .

A second approach of implicitly incorporating the time-cost of the fidelities is to take the ratio of the compute times with respect to the target fidelity. This approach is motivated by posing the question, what amount of training data used at a specific fidelity would cost the same as the training data used at the target fidelity. Once again, the nearest integer value is considered. This leads to the definition of $\theta_F^f := \lfloor T^F / T^f \rfloor$ for all $f < F$. As for the case of θ_{f-1}^f , the reference molecule was chosen to be o-HBDI. This leads to scaling factors $\theta_f^F = \{9, 3, 2, 1\}$ for increasing fidelity. Since the SVP fidelity is scaled by a factors of 1, as discussed earlier, one additional training samples was added each time to maintain the multifidelity structure required for MFML. As an example, consider the case for $N_{train}^{TZVP} = 2$. Then the training samples at the different fidelities would be $\{108, 12, 4, 2 + 1, 2\}$. This formulation of scaling factors is hereon associated with θ_f^F .

2.5 Error Contours of MFML

The prediction error of the different ML and MFML models assessed in this work are given as mean absolute errors (MAE) which is calculated over the holdout test set as:

$$MAE = \frac{1}{N_{test}} \sum_{q=1}^{N_{test}} \left| P_{ML} \left(\mathbf{X}_q^{ref} \right) - y_q^{ref} \right|. \quad (8)$$

Due to the multifidelity data structure a simple cross validation approach cannot be used. Instead, the MAE of the MFML models is calculated for a 10-run average as proposed and implemented in ref. [17], which accounts for the nested multifidelity data structure. For most ML approaches, the MAE is reported for increasing training set sizes, thereby resulting in a learning curve. The learning curves is used as an indicator of the ability of the ML model to predict over unseen data. Learning curves form a major part of the analysis offered in this work. In addition to the usual MAE versus training samples learning curves, this work also studies the MAE versus cost of generating training data for the multifidelity model as first proposed and implemented in ref. [18] for excitation energies.

The analysis of the learning curves for the different values of γ (see section 3.1 and section 3.2) indicate that the MFML training data structure needs only very little training samples at the higher fidelity. The contribution of each fidelity and the number of training samples at each fidelity is more complex than just the QC-time cost of the fidelity. In interest of studying the individual contribution of each fidelity and the diverse training samples choices at each fidelity, this work introduces a new error metric, namely, error contours. As a conceptual extension of learning curves, error contours of MFML report MFML model error as a function not simply of training samples chosen at a single fidelity but as a function of training samples, N_{train}^f and N_{train}^{f+1} , chosen at two consecutive fidelities, f and $f + 1$. In other words, the error contour is the MAE of the MFML model by varying the training samples at two fidelities simultaneously. Since this work uses the QeMFi dataset that contains five fidelities, the error contours of MFML are studied for the following fidelity pairs: TZVP-SVP, SVP-631G, 631G-321G, and 321G-STO3G. Since the error contours are a function of two variables, N_{train}^f and N_{train}^{f+1} , they are reported as contour plots. Herein, error contours of MFML are discussed only for $\gamma = 2$. The error contours give a better view into the contribution of a

multifidelity data structure to model accuracy for a given target fidelity. The investigation of error contours for each fidelity pair indicates, in some sense, the weighted contribution of those fidelities to the overall model. A better understanding of this contribution will aid the choice of N_{train}^f for each fidelity that constitutes the MFML model.

2.6 The Γ -Curve

The study of the error contours in section 3.3 indicates that the multifidelity data structure can provide a high-accuracy model with a much lower number of costly training samples than the conventional MFML data structure approach. Coupled with the results of studying the learning curves for different scaling factors (see sections 3.2 and 3.3), a new multifidelity approach is proposed: the Γ -curve.

In this approach, a fixed number of training samples are chosen at the highest fidelity, N_{train}^{TZVP} . An o-MFML model is built with $\gamma = 2$. The cost of the training data is noted along with the model error over the holdout test set. For the next step of this curve, instead of varying N_{train}^{TZVP} , γ is increased by an integer value. This curve is identified as $\Gamma(N_{train}^{TZVP})$ -curve and is a measure of MAE versus time-cost of training data of the multifidelity model for varying γ . For example, if one were to set $N_{train}^{TZVP} = 2$, $f_b : 321G$, then the $\Gamma(2)$ -curve would be built with the first multifidelity training data structure (in increasing fidelity) as $\{2^3 \cdot 2, 2^2 \cdot 2, 2^1 \cdot 2, 2\}$. The next point would be built with a training data structure of $\{3^3 \cdot 2, 3^2 \cdot 2, 3^1 \cdot 2, 2\}$ and so on. In general, for a $\Gamma(N_{train}^{TZVP})$ -curve, the training data structure for $f : b$ 321G is given as $\{\gamma^3 \cdot N_{train}^{TZVP}, \gamma^2 \cdot N_{train}^{TZVP}, \gamma^1 \cdot N_{train}^{TZVP}\}$. For reasons explained in section 3.2 and section 3.3, the STO3G baseline is not considered. Herein, the $\Gamma(\cdot)$ -curve is studied for $N_{train}^{TZVP} \in \{2, 8, 64\}$ to further assess the multifidelity structure of training data and evaluate the limits of the multifidelity approach. Since there is no trivial way to express the number of training samples used at a certain fidelity and relate it to the MAE of the model, the $\Gamma(\cdot)$ -curve is plotted only as MAE versus multifidelity training data generation cost.

3 Results

This section presents the analysis of varying the scaling factor for MFML and o-MFML. The results are presented in two major formats. First, standard learning curves of MAE versus number of training samples used at the highest fidelity of TZVP are presented. Following this, the model error is assessed a function of the time-cost of generating the training data for the model. This assessment from ref. [18] informs of the effectiveness of the diverse models that are studied in this work. Once these results are interpreted, error contours of MFML as described in section 2.5 are studied.

3.1 Learning Curves

The primary assessment of the effect of different scaling factors is carried out using learning curves for the resulting MFML and o-MFML models. These learning curves are shown in Fig. 2 for different scaling factors. In all cases, the scaling factors are constant across the different fidelities as explained in section 2.4. The top row of the figure depicts the learning curves for MFML while the bottom row corresponds to the o-MFML models. The learning curves are shown for varying baseline fidelities. A single fidelity KRR learning curve is also shown for reference. The MAEs are reported in units of cm^{-1} for the excitation energies of the QeMFi dataset.

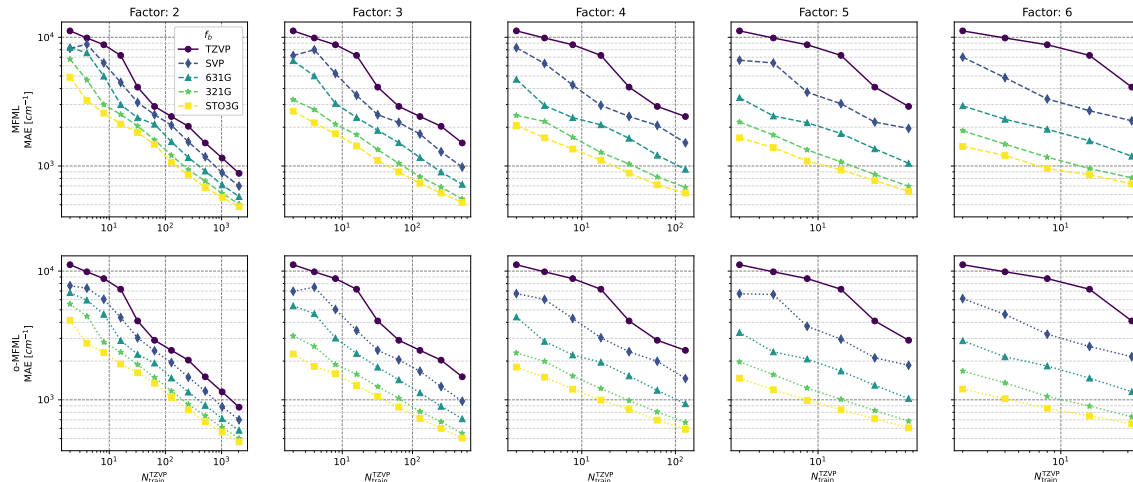


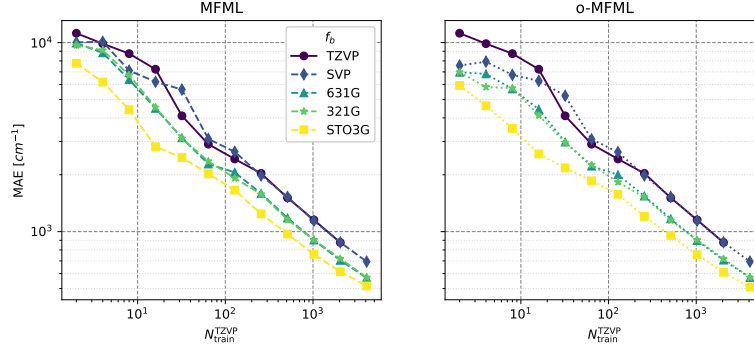
Fig. 2: Multifidelity learning curves for the prediction of excitation energies taken from the QeMFi dataset. The top row corresponds to the MFML models while the bottom row is for the o-MFML models. Different fixed scaling factors are used to scale the data across each fidelity in the multifidelity models as explained section 2.4. The scaling factors are reported on the top of each column.

In Fig. 2, the first column shows the learning curves for the scaling factor of 2. This is the original scaling factor used in ref. [17, 18, 24] and is used as a reference to evaluate the other scaling factors against. Within these reference results, one observes that the addition of cheaper baselines results in a constantly lowered offset of the learning curves. The interpretation from the lowered offsets is that similar models errors can be achieved with lower number of training samples at the target fidelity with the addition of cheaper fidelities. With the cheapest fidelity, STO3G, being added to the multifidelity model, one observes an error of 10^3 cm^{-1} with around 200 training samples at TZVP.

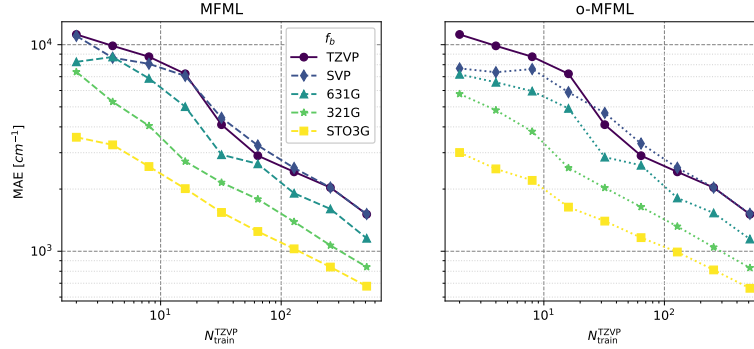
In comparison to this, an increase of the scaling factor, γ , provides MFML models that achieve similar errors for lower number of training samples at TZVP. A comparison of the MFML models built with different values of γ for the STO3G baseline fidelity are shown in Fig. 4. For example with a scaling factor of 3, the STO3G baseline MFML model achieves an error of 10^3 cm^{-1} with $N_{train}^{TZVP} \sim 40$. With a scaling factor of 6, the number of training samples at TZVP needed to achieve this same error is lowered further to about 8. The learning curves for o-MFML also indicate the same across varying scaling factors. There is little difference between the learning curves for MFML and o-MFML. This could be due to the MFML combination being already optimal for this multifidelity data structure as has been argued in ref. [17]. There is however, slight improvement in all cases of o-MFML and it does result in reduced MAEs across the different scaling factors.

From these results it appears that a higher number of training samples with cheaper fidelities improves the predictive capabilities of the MFML and o-MFML models. One possible reason for this could be that the use of larger data at the cheaper fidelities results in more information about the overall multifidelity structure being included into the MFML models.

In addition to the fixed scaling factors across fidelities, two special cases of scaling factors were introduced in section 2.4 based on the QC compute time of each fidelity. These were denoted by



(a) Scaling factors, $\theta_{f_{-1}}^f$, between fidelities chosen as ratios of the QC compute time of subsequent fidelities. Single fidelity KRR at TZVP is also shown for reference.



(b) Scaling factors, θ_f^F , between fidelities selected as ratios of the QC compute time of that fidelity to the compute time of TZVP, that is the target fidelity.

Fig. 3: MFML and o-MFML learning curves time informed scaling factors (see section 2.4). The two time informed scaling factors are described in detail in section 2.4. Single fidelity KRR learning curves are also provided for reference. The legend describes the baseline fidelity, f_b , of the multifidelity model.

$\theta_{f_{-1}}^f$ and θ_f^F as explained in section 2.4 in detail. Learning curves were generated for both MFML and o-MFML models for both these cases. The results are shown in Fig. 3 for both scaling factor cases with various baseline fidelities. The single fidelity KRR learning curves is also depicted for reference.

Fig. 3a depicts the results for $\theta_{f_{-1}}^f$ with the left pane for MFML and right pane for o-MFML. As explained in section 2.4, these scaling factors are based on the ratio of QC-compute times of subsequent fidelities - namely between TZVP and SVP, and between 631G and 321G - this scaling was observed to be 1. It is anticipated that these fidelities will not significantly improve the MFML models since there is very little additional information that is being added to the model. Indeed, as seen in Fig. 3a, the multifidelity model built with SVP baseline does not provide any improvement over the single fidelity KRR. This is due to the fact that the number of training samples at both fidelities are nearly identical, only different by 1 sample, due to the

scaling factor. This same observation can be made for the learning curves with 321G as baseline fidelity. With 631G and STO3G baselines, however, one observes improvement of the MFML and o-MFML models. With the STO3G baseline, MFML and o-MFML reach an error of 10^3 cm^{-1} with roughly 500 training samples at TZVP.

Similarly, Fig. 3b reports the learning curves for θ_f^F . The left-pane shows the results for MFML, while the right pane shows those for o-MFML. The SVP baseline fidelity once again shows very little improvement over the single fidelity KRR due to the scaling factor being unity (see section 2.4). However, each additional cheaper baseline fidelity, results in lowered offsets of the corresponding learning curves. With $N_{train}^{TZVP} \sim 100$, the multifidelity models with the STO3G baseline result in MAE of 10^3 cm^{-1} .

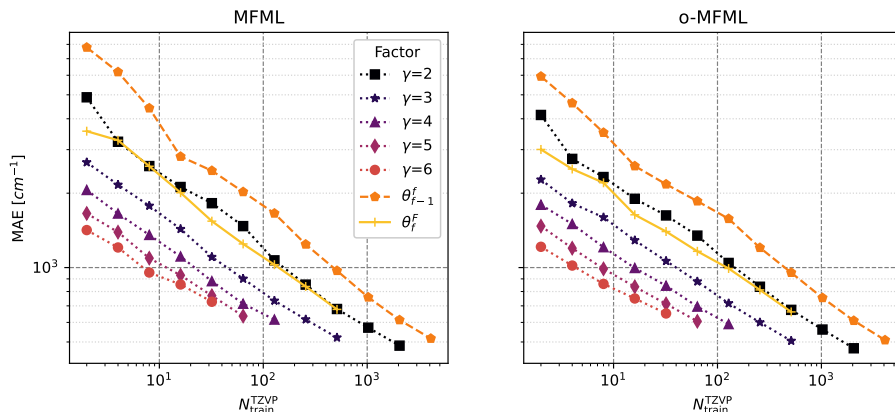


Fig. 4: Comparison of learning curves for fixed scaling factors γ , θ_{f-1}^f , and θ_f^F with f_b : STO3G. The x-axis reports the number of training samples used at the highest fidelity, that is, TZVP. Both MFML and o-MFML models are compared. Increasing values of γ result in a constant lowered offset of the learning curves. The cost informed scaling factors show a higher value of MAE.

To aid comparison of the different scaling factors discussed so far, Fig. 4 depicts the learning curves for the MFML and o-MFML models built with the STO3G fidelity as baseline. The various factors are delineated in the legend of the plot. This plots shows that increasing values of γ result in a lowered constant offset of the learning curves. In contrast, the multifidelity models built with time-informed scaling factors, θ_{f-1}^f and θ_f^F both show the highest model error. This observation is consistent for both MFML and o-MFML models as can be seen from the two plots shown in Fig. 4. Furthermore, the o-MFML models show lower errors than the MFML counterparts for all the cases as seen in table 1 which reports the MAEs for the MFML and o-MFML models with various scaling factors for the STO3G baseline for $N_{train}^{TZVP} = 2^5$ for ready reference. This training set size is chosen so that there is uniform comparison between the different scaling factors. The behavior of the MFML models with increasing γ is in some sense expected since an increasing value of the scaling factor implies an increased amount of training data, albeit only at the cheaper fidelities. This could be one potential reason to explain the lowered offsets that are observed. An increased amount of training samples at the lowered fidelities, due to the nested structure of the

Factor	MFML	o-MFML
2	2044	1879
3	1339	1267
4	1036	988
5	860	826
6	809	738
θ_{f-1}^f	3112	2959
θ_f^F	2151	2028

Table 1: MAE in cm^{-1} rounded off to nearest integer of MFML and o-MFML models built with the STO3G baseline fidelity for $N_{train}^{TZVP} = 2^5$. This allows for a uniform comparison of the model accuracy not just between MFML and o-MFML but also across the scaling factors that are studied in this work. Notice that the learning curve for $\gamma = 6$ only goes up to $N_{train}^{TZVP} = 2^5$ and therefore this is chosen as a comparison point for all other curves.

multifidelity training data, could impart meaningful information about the conformational phase-space and its relation to the excitation energies. The limited improvement that is seen from the learning curves of θ_{f-1}^f and θ_f^F , which both had a much larger number of training samples at the cheapest fidelity in comparison to the other fidelities, could be due to the lack of sufficient training data in the fidelities that lie between the baseline and target fidelities. Furthermore, the value of θ_{f-1}^f for the SVP and 321G fidelities was 1 which did not provide any additional information to the MFML model as was pointed out in the discussion for Fig. 3a. This in turn affects the overall model that is built with the STO3G baseline fidelity. A similar argument can be made for why the MFML model with θ_f^F has limitations. Regardless, the MFML model built with θ_f^F does in fact achieve model MAE that are comparable to the MFML model built with $\gamma = 2$.

The results for fixed scaling factors, γ , indicate that a higher γ results in a lower model error, or, smaller number of training samples at the costly target fidelity are needed. For the time-informed scaling factors, it was seen that these do not perform as well as was anticipated. However, one must be cautious about the results from Fig. 2 and Fig. 3 before considering them to be improvements over the conventional MFML method with $\gamma = 2$. Since one uses much more training samples at the cheaper fidelities as one increases the value of γ , the cost of generating training data needs to be assessed to better understand the cost-accuracy trade-off in these multifidelity models. In interest of such an analysis, the time-cost of generating training data versus model MAE are discussed in the next section. Although the MFML and o-MFML models show similar MAEs, only o-MFML models are discussed hereon. This is due to the observation of ref. [17] that the o-MFML method provides a superior model even in cases of poor data distribution of the cheaper fidelities. That is, in the case of a poor data distribution, the o-MFML provides the better model in comparison to MFML. Since all o-MFML models use the same validation set, the cost of generating the validation set is not included in the time-analysis plots.

3.2 Time Benefit Analysis

As presented in refs. [18, 20], a good assessment of multifidelity methods is the study of model error versus the time to generate the training samples for the model. In interest of such a study, the MAE versus training data generation time are studied for the just discussed test cases. The time to generate data for a multifidelity model is the sum over the times for generation of all the

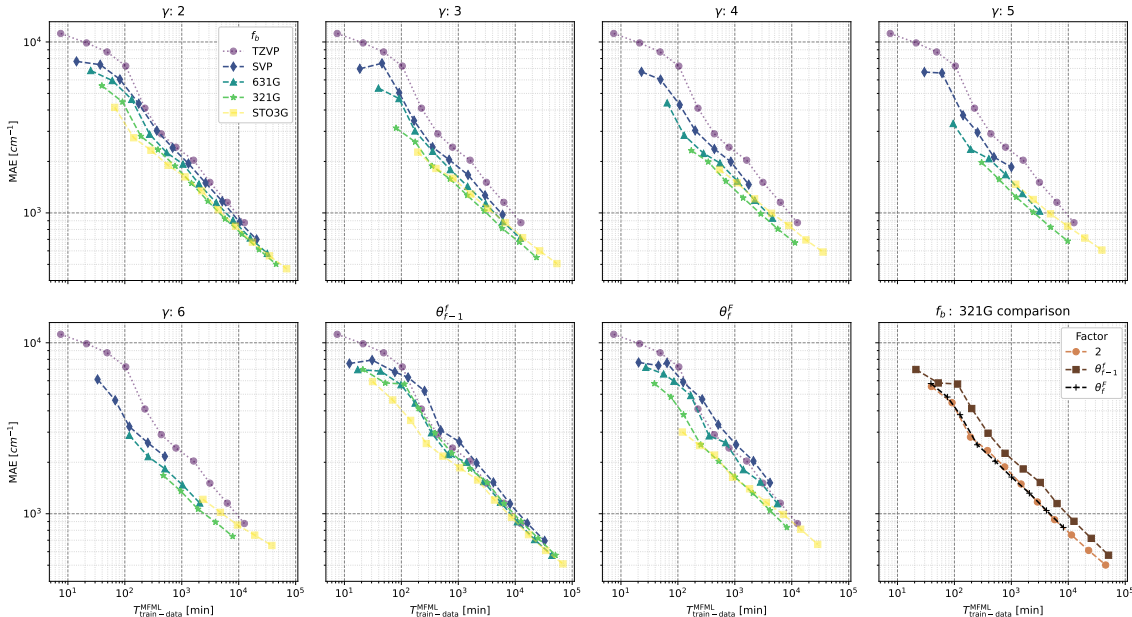


Fig. 5: Time to generate training data versus MAE of the corresponding o-MFML model for the diverse scaling factors studied. The different scaling factors used are denoted as sub-titles. The MAE is reported in cm^{-1} and the time in minutes. The single fidelity KRR case is also depicted for reference. As one increases the scaling factors across the fidelities, one observes that the learning curves of the MFML models shifts further due to the larger amount of training samples used. The two cases of θ_{f-1}^f and θ_f^f are explained in section 2.4. The bottom-right corner plot compares the o-MFML curves for the 321G baseline for the two time-informed scaling factors and the case of $\gamma = 2$.

training samples used at all fidelities that form the multifidelity model. That is, $T_{train-data}^{MFML} := \sum_{f_b \leq f \leq F} N_{train}^f \cdot T_{QC}^f$ where N_{train}^f is the number of training samples used at some fidelity f , and T_{QC}^f is the corresponding single-point QC-compute time for that fidelity. The QC-compute times recorded in the QeMFi dataset are those for a single-core computation and are provided for each fidelity for each molecule type [20].

The MAE versus $T_{train-data}^{MFML}$ plots for the various scaling factors are shown in Fig. 5 for o-MFML. Only o-MFML is shown since it has a lower error compared to MFML for all the cases (see Figs. 2 and 3). The MAE and the time axes are both presented in log-scaled values. The axes of the plots are scaled identically for easy comparison among the different scaling factors. The bottom-right corner plot compares the time-cost based scaling factors to the case of $\gamma = 2$ for the MFML model built with f_b : 321G and not for the cheapest STO3G baseline for reasons discussed below.

For the different cases of scaling factors shown in Fig. 5, it can be seen that the addition of cheaper baselines helps achieve a specific model accuracy with less time cost to generate the training data. In general, fixing a specific MAE, one can see that the curves of the cheaper baseline achieve this error earlier with respect to the time axis. Alternatively, if one were to set a time budget and

draw a vertical line at that value (as on the x-axis), then the cheaper baseline models result in lower MAEs than the single fidelity KRR model. The case of STO3G baseline is an exception. For all scaling factors, the addition of the STO3G baseline does not provide significant improvement of the model. In fact, it increases the training data generation cost. The STO3G energies do not provide major improvement to the o-MFML model over the 321G baseline. This could be due to poor data distribution that has previously been noted for the STO3G fidelity for excitation energies of molecules [17–19]. The time-cost versus MAE plots make this evident. Although the analysis of conventional learning curves from section 3.1 indicated that the STO3G baseline fidelity improved the MFML model, these time-cost plots indicate that this comes at a cost which supersedes the MAE improvement that is observed. However, consider the case of the special scaling factors θ_f^F , which are decided by the ratio of the QC-compute times of a fidelity f to the QC-compute time of the target fidelity F . For some portions of learning curve for $f_b = \text{STO3G}$, o-MFML does provide lower errors as is expected from such multifidelity models [17]. This could indicate that the use of o-MFML could improve the model accuracy even for the cases of poor data distribution as seen in the STO3G fidelity. For the o-MFML models that are built with the 32G baseline fidelity, the time benefit of the multifidelity approach becomes all the more perceptible across the various scaling factors. For instance, in the case of $\gamma = 3$, the o-MFML model results in an error of $\sim 2,000 \text{ cm}^{-1}$ with a time cost of ~ 200 minutes. The KRR model achieves a similar error with a time-cost of $\sim 1,000$ minutes. This indicates a time benefit of about 5 times with this baseline fidelity for $\gamma = 3$. Similarly, for $\gamma = 5$, the KRR model achieves an error of $\sim 2,000 \text{ cm}^{-1}$ with a time cost of $\sim 2,000$ minutes while the o-MFML model achieves a similar error for a time cost of ~ 300 minutes resulting in a time benefit of about 6 times. Similar observations can be made for the other values of γ . The time benefit is less pronounced for the cases of θ_{f-1}^f and θ_f^F but is still present for $f_b : 321\text{G}$.

While each scaling factor does improve the time-cost needed to achieve a certain MAE vis-à-vis the single fidelity KRR, it is also important to see which scaling factor performs better with respect to the others for a given baseline fidelity. The bottom-right plot of Fig. 5 compares the time-cost versus MAE curves of MFML models for $\gamma = 2$, θ_{f-1}^f , and θ_f^F for the baseline fidelity of 321G. The STO3G baseline is not considered due to its poor distribution. These specific scaling factors are chosen to better understand the standing of the time-informed scaling factors with respect to the fixed scaling factors. The time-cost versus MAE of different γ are compared in Fig. 7 in light of the discussion about the $\gamma(\cdot)$ -curves. This comparison in Fig. 5 for the 321G fidelity shows that the fixed scaling factor of $\gamma = 2$ performs better than both the time-cost informed scaling factors see section 2.4. The MFML model built with θ_f^F does perform only as well as that built with $\gamma = 2$, which is the default set-up for MFML. This could indicate that just the QC-compute time-cost information might not suffice to select the training samples at each fidelity. It could be that the model accuracy and multifidelity training structure relation is more complex than just accounting for the QC-compute cost. To better understand how each fidelity and the number of training samples at each fidelity contribute to the overall model error, the next section studies a new error metric, error contours (see section 2.5 for details). This is intended to give a better view into the inner mechanisms of the multifidelity data structure in building a MFML model.

3.3 Multifidelity Error Contours

The time versus MAE results for different scaling factors hint that one might not necessarily need many training samples at the target fidelity. This would imply that one could build a cheap multifidelity model with a large number of training samples at the cheaper fidelities and then ‘raise’ it

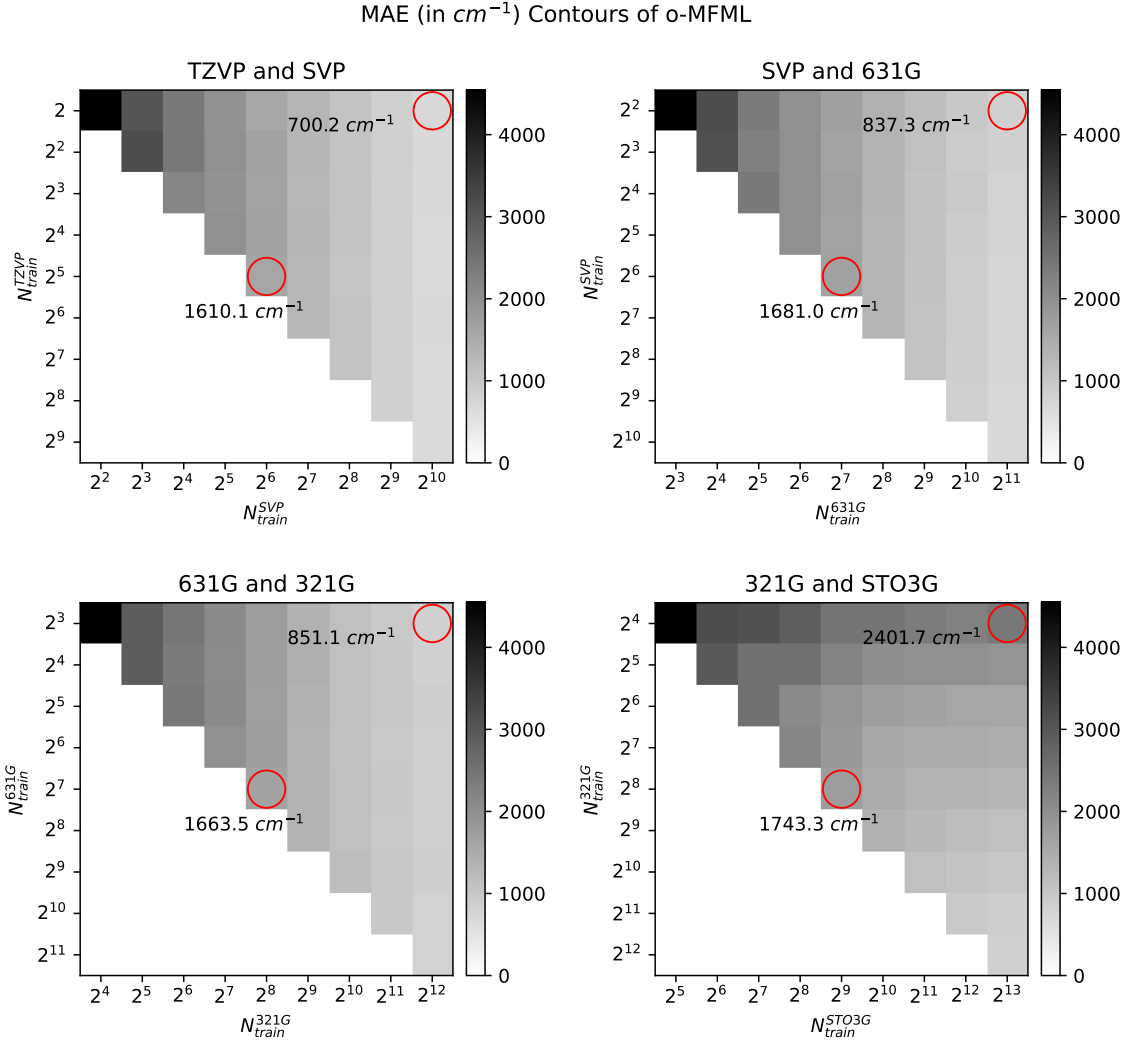


Fig. 6: Excitation energy prediction errors with o-MFML for different training samples at different fidelities. The details of the method are explained in section 2.4 for each case. In each plot, the vertical axis depicts the number of training samples used at the costlier fidelity, f , while horizontal axis reports the training samples used at the cheaper fidelity $f - 1$. The resulting error for the o-MFML model with the specific choice of training samples used at fidelity f and $f - 1$ are depicted as the error contours. Here, the MAE are depicted as contour plots for different training samples spanned across two fidelities. The MAEs are reported in cm^{-1} . Two specific MAEs are enumerated for all 4 cases: first, that for the smallest training set size at the higher fidelity, f , and the largest training set size at $f - 1$; second, for the case where the training sample at f and $f - 1$ have the scaling factor of 2.

to the target fidelity with an exceptionally small number of training samples at the target fidelity. This can be further studied with the error contours of multifidelity. These contours involve studying the model prediction error by varying the training sizes along fidelity f and $f - 1$ for all $f \leq F$. As was discussed in section 2.4, this is performed for consecutive fidelity pairs TZVP-SVP, SVP-631G, 631G-321G, and 321G-STO3G.

Fig. 6 illustrates the multifidelity error contours of o-MFML for different fidelity pairs for $\gamma = 2$. Consider the top-left plot corresponding to the TZVP-SVP fidelity pair. The y-axis denotes the number of training samples used at TZVP, while the x-axis depicts the number of training samples used at the SVP fidelity. The colors of the plot itself correspond to the MAE. In the usual o-MFML approach, the number of training samples used at SVP with respect to the number of training samples used at TZVP would be scaled by the factor γ (in this case by 2). However, for this set-up there is no trivial scaling of training data that is carried out. Instead, the multifidelity model is built with a specific selection of training samples. For example, take the case for $N_{train}^{TZVP} = 2$ and $N_{train}^{SVP} = 2^{10}$ which is marked by the top-corner red circle. The MAE reported here is for a multifidelity model that is built with the following multifidelity training structure (with increasing fidelity): $\{2^3 \cdot 2^{10}, 2^2 \cdot 2^{10}, 2 \cdot 2^{10}, 2^{10}, 2\}$. In other words, the scaling factor is only applied for the fidelities that are not studied as part of the error contour. This specific multifidelity model reports an MAE of about 700 cm^{-1} . In contrast, in the usual o-MFML the training data structure would be $\{2^4 \cdot 2, 2^3 \cdot 2, 2^2 \cdot 2, 2 \cdot 2, 2\}$, this is the block that corresponds to $(N_{train}^{SVP} = 2^2, N_{train}^{TZVP} = 2)$ on the plot. The accompanying color-bar depicts that this regular o-MFML model has a high MAE $\sim 4,000 \text{ cm}^{-1}$. In general, the diagonal of the contour plot depicts the regular o-MFML model which is identified in the learning curves of Fig. 2 for $\gamma = 2$. The MAE for $(N_{train}^{SVP} = 2^6, N_{train}^{TZVP} = 2^5)$ is highlighted as well reporting a MAE of about $1,610 \text{ cm}^{-1}$ which is almost twice as what is observed for $(N_{train}^{SVP} = 2^2, N_{train}^{TZVP} = 2)$. This is a remarkable observation in that simply using two training samples at TZVP while increasing the training size at the lower fidelities results in a model that is more than twice as accurate. Furthermore, the MAE for the block $(N_{train}^{SVP} = 2^2, N_{train}^{TZVP} = 2)$ is similar to the model block $(N_{train}^{SVP} = 2^{10}, N_{train}^{TZVP} = 2^9)$. In general, it is seen that a lower number of TZVP training samples with a larger training set size at the cheaper fidelities results in more accurate multifidelity model.

Similar observations and inferences can be made for the error contour for the SVP-631G fidelity pair as seen on the top-right plot of Fig. 6. In this set-up, consider the top right corner which is marked with a circle. This is identified as $(N_{train}^{631G} = 2^{11}, N_{train}^{SVP} = 2^2)$ and has the following multifidelity data structure (with increasing fidelity): $\{2^{13}, 2^{12}, 2^{11}, 2^2, 2\}$. As in the previous case, the training data scaling is only applied to the fidelities that are not studied as part of the error contour. This mode reports a MAE of about 837 cm^{-1} . Once again, the diagonal of the contour plot corresponds to the regular o-MFML model. Consider then, the block identified by $(N_{train}^{631G} = 2^6, N_{train}^{SVP} = 2^7)$ which has a training data structure (in increasing order of fidelity): $\{2^9, 2^8, 2^7, 2^6, 2^5\}$. This regular o-MFML model reports an error of around $1,681 \text{ cm}^{-1}$, almost twice as much as for the previous one. The overall contour plot reveals that the use of very few training samples at SVP paired with a larger number of training samples at the lower fidelities results in MAEs that are comparable to the cases where one would use a lot more training samples at the SVP fidelity. In particular, this form of *flattening* out the multifidelity training structure by using few training samples at the top fidelities and increasing the training samples at the cheaper fidelities, outperforms the regular o-MFML model (which are the diagonal blocks of the error contour).

Similar observations are made for the 631G-321G and 321G-STO3G pairs of fidelities which are seen in the bottom row of Fig. 6. It is interesting to note, however, that the 321G-STO3G error

contours do not follow the same trend as the others. Using very little 321G training samples and increasing the training samples at the STO3G fidelity does not result in lower MAE as seen from the top-corner red marker error being $\sim 2400 \text{ cm}^{-1}$ while the center marker reporting an error of $\sim 1740 \text{ cm}^{-1}$. This is once again explained by the poor data distribution that has previously been reported for the STO3G fidelity [17–19].

The error contours for the multifidelity model hint at an interesting mechanism in the MFML approach. Based on the behavior of the model error as discussed above, it appears that one does not necessarily need to use many training samples at the higher fidelities, in particular at the target fidelity. This is indeed something that has been previously hinted at in ref. [5] using the optimization procedure for h-ML albeit with a larger number of training samples at the target fidelity. However, a thorough investigation of the multifidelity structure such as that performed in Fig. 6 reveals that not only can a multifidelity model be built with low number of training samples at the costlier fidelities, but that this number is far smaller than what would be anticipated in the general MFML and similar methods. The error contours indicate that there is still a great deal of information available at the cheaper fidelities which only need to be ‘raised up’ to the target fidelity with a surprisingly small number of training samples. With such an understanding of the multifidelity training structure, one can begin to think of ways to select training samples at the different fidelities that need not necessarily follow the concept of a scaling factor between the fidelities. Furthermore, the results of varying γ from Fig. 5 hint at a possible approach which is pursued in the following section.

3.4 Γ -curves

The contour plots of Fig. 6 provide an interesting observation about MFML. One can potentially build cheaper multifidelity models by limiting the training samples used at the expensive fidelities and then proceeding to add cheap fidelity data to the multifidelity model.

Consider first the left-hand side plot of Fig. 7 which shows the MAE curves of o-MFML with $f_b : 321\text{G}$ for the different γ studied in this work for comparison. An inset plot is provided which zooms into the region between 1,000-3,000 minutes to show the different curves clearly. In addition, a new curve as introduced in section 2.6, the ‘ $\Gamma(2)$ -curve’ is depicted in the plot. The $\Gamma(2)$ -curve is essentially the case where the number of training samples at TZVP are constrained to 2 but the remaining multifidelity data structure is allowed to grow as per the scaling factor γ . That is, the $\Gamma(2)$ -curve is built with the first point of the curves for the different γ values. In some sense, this translates into it being a learning curve not as a function of N_{train}^{TZVP} but rather of γ . From Fig. 7, it becomes evident that even for as little as 2 training samples at the highest fidelity, if one adds cheaper data to the multifidelity model - which corresponds to increasing the value of γ without increasing N_{train}^{TZVP} - the error of the o-MFML model decreases. For the same time-cost of a conventional o-MFML model built with $\gamma = 2$, if one were to chose the models along the $\Gamma(2)$ -curve, a lower MAE can be achieved. The $\Gamma(2)$ -curve in Fig. 7 shows data points for up to $\gamma = 10$ where the multifidelity training data structure (for increasing fidelity) is: $\{20000, 2000, 200, 20, 2\}$. In the inset of the plot, one observes that the $\Gamma(2)$ -curve results in errors that are lower than the o-MFML learning curves for fixed γ . However, the $\Gamma(2)$ -curve converges to the o-MFML model built with $\gamma = 6$. One potential reason for this could be the saturation of the multifidelity model built along the $\Gamma(2)$ -curve. Due to a very large number of training samples at the cheaper fidelities (for instance, $2 \cdot 10^4$ at 321G for the last point on the $\Gamma(2)$ -curve), the model is no longer able to clearly learn the correction between SVP and TZVP.

The right-hand plot of Fig. 7 further investigates this saturation by comparing ΓN_{train}^{TZVP} -curves for $N_{train}^{TZVP} \in \{2, 8, 64\}$. The y-axis reports the MAE in cm^{-1} while the x-axis denotes the time-cost in minutes to generate the training data used in the multifidelity models. An inset is provided for the interval between $10^3 - 10^4$ minutes for a better view of the $\Gamma(\cdot)$ -curves. The o-MFML learning curve for $\gamma = 2$ is provided for reference.

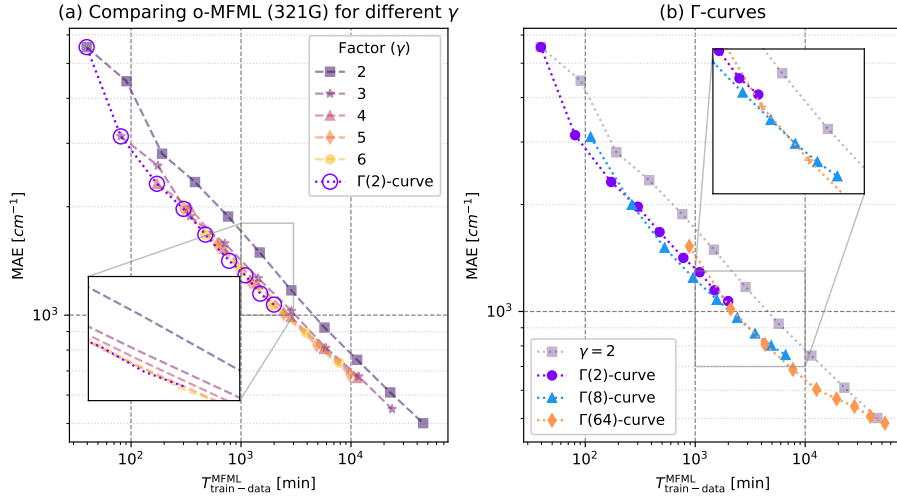


Fig. 7: (a) Time to generate training data and corresponding o-MFML model error as MAE in cm^{-1} for constant scaling factors, γ used in this study. An inset between 1,500-3,000 minutes is provided for the comparison of the curves for all γ studied in this work to readily compare in regions that are too crowded to be observed in the main plot. (b) MAE versus time-cost for different $\Gamma(N_{train}^{TZVP})$ -curves. Increasing the number of training samples at TZVP improves the model accuracies along the $\Gamma(\cdot)$ -curves with a saturation observed towards the end of each curve.

4 Conclusions and Outlook

This work discusses the concept of scaling for the number of training data across different fidelities for MFML and o-MFML in the prediction of excitation energies of the QeMFi dataset. Constant scaling factors, γ , were studied along with QC-calculation time-cost informed scaling factors, θ_{f-1}^f and θ_f^f . It is seen in the results that the use of constant scaling factors, γ , is effective with a higher value of γ resulting in lower model errors for reasonable time-cost of generating training data. A new error metric, the error contour of MFML, was introduced and results discussed for the prediction of first vertical excitation energies of the QeMFi dataset. Such an analysis revealed that the data requirements for MFML-like methods is not as trivial as has been previously employed. In fact, one can achieve similar model accuracies with much less costly training samples if one increases the number of training samples at the lower end of the multifidelity data structure. The error contours revealed that one could potentially use as little as 2 training sample at the target fidelities and

achieve exceptional model accuracy if the subsequent fidelities used a larger number of training samples in comparison to MFML models built with some γ . This was systematically studied with the newly introduced Γ -curve for a fixed number of training samples at the target fidelity and an increasing value of γ . The models built in this fashion were shown to be time-cost efficient over conventional MFML approach.

These results provide a window into the inner mechanisms of MFML-like methods allowing for a better understanding of how they can be employed for accurate predictions of excitation energies with low cost of training data generation. Future research over this could include algorithms that optimally select the number of training samples to be used at each fidelity. Further work could involve extending this to other time-based scaling factors which also take into account the error reduction that each additional training sample contributes to the overall multifidelity model. This would further improve the scope of application for the multifidelity methods discussed herein.

Data Availability. The data used in this study was taken from the QeMFi dataset which can be found in [this ZENODO data repository](#). The programming scripts used for this study can be openly accessed at [this GitHub repository](#).

Acknowledgments. The authors acknowledge support by the DFG through the project ZA 1175/3-1 as well as through the DFG Priority Program SPP 2363 on “Utilization and Development of Machine Learning for Molecular Applications – Molecular Machine Learning” through the project ZA 1175/4-1. The authors would also like to acknowledge the support of the ‘Interdisciplinary Center for Machine Learning and Data Analytics (IZMD)’ at the University of Wuppertal.

Disclosure of Interests. The authors declare that there is neither a conflict of interest nor any competing interests.

References

1. Jörg Behler. Constructing high-dimensional neural network potentials: a tutorial review. *Int. J. Quantum Chem.*, 115:1032–1050, 2015. URL: <https://onlinelibrary.wiley.com/doi/abs/10.1002/qua.24890>, doi:10.1002/qua.24890.
2. Keith T. Butler, Daniel W. Davies, Hugh Cartwright, Olexandr Isayev, and Aron Walsh. Machine learning for molecular and materials science. *Nature*, 559(7715):2336–2347, 2018. doi:10.1038/s41586-018-0337-2.
3. Pavlo O Dral. Quantum chemistry in the age of machine learning. *J. Phys. Chem. Lett.*, 11:2336–2347, 2020. doi:10.1021/acs.jpcllett.9b03664.
4. Pavlo O. Dral and Mario Barbatti. Molecular excited states through a machine learning lens. *Nat. Rev. Chem.*, 5(6):388–405, 2021. doi:10.1038/s41570-021-00278-1.
5. Pavlo O Dral, Alec Owens, Alexey Dral, and Gábor Csányi. Hierarchical machine learning of potential energy surfaces. *J. Chem. Phys.*, 152:204110, 2020. doi:10.1063/5.0006498.
6. K. E. Fisher, M. F. Herbst, and Y. M. Marzouk. Multitask methods for predicting molecular properties from heterogeneous data. *The Journal of Chemical Physics*, 161(1):014114, 07 2024. arXiv:https://pubs.aip.org/aip/jcp/article-pdf/doi/10.1063/5.0201681/20030605/014114_1_5_0201681.pdf, doi:10.1063/5.0201681.
7. Helmut Harbrecht, Michael Peters, and Markus Siebenmorgen. Combination technique based k-th moment analysis of elliptic problems with random diffusion. *J. Comput. Phys.*, 252:128–141, 2013. URL: <https://www.sciencedirect.com/science/article/pii/S0021999113004373>, doi:10.1016/j.jcp.2013.06.013.

8. Markus Hegland, Brendan Harding, Christoph Kowitz, Dirk Pflüger, and Peter Strazdins. Recent developments in the theory and application of the sparse grid combination technique. *SPPEXA 2013-2015*, pages 143–163, 2016. doi:10.1007/978-3-319-40528-5_7.
9. Sergei Manzhos and Tucker Jr. Carrington. Neural network potential energy surfaces for small molecules and reactions. *Chem. Rev.*, 121(16):10187–10217, 2021. PMID: 33021368. doi:10.1021/acs.chemrev.0c00665.
10. Frank Noé, Alexandre Tkatchenko, Klaus-Robert Müller, and Cecilia Clementi. Machine learning for molecular simulation. *Annu. Rev. Phys. Chem.*, 71:361–390, 2020. doi:10.1146/annurev-physchem-042018-052331.
11. Abhirup Patra, Rohit Batra, Anand Chandrasekaran, Chiho Kim, Tran Doan Huan, and Rampi Ramprasad. A multi-fidelity information-fusion approach to machine learn and predict polymer bandgap. *Comput. Mat. Sci.*, 172:109286, 2020. URL: <https://www.sciencedirect.com/science/article/pii/S0927025619305853>, doi:10.1016/j.commat.2019.109286.
12. Raghunathan Ramakrishnan, Pavlo O. Dral, Matthias Rupp, and O. Anatole von Lilienfeld. Big Data Meets Quantum Chemistry Approximations: The δ -Machine Learning Approach. *J. Chem. Theory Comput.*, 11:2087–2096, 5 2015. doi:10.1021/acs.jctc.5b00099.
13. Christoph Reisinger. Analysis of linear difference schemes in the sparse grid combination technique. *IMA J. Numer. Anal.*, 33:544–581, 09 2013. doi:10.1093/imanum/drs004.
14. Matthias Rupp, Alexandre Tkatchenko, Klaus-Robert Müller, and O. Anatole von Lilienfeld. Fast and accurate modeling of molecular atomization energies with machine learning. *Phys. Rev. Lett.*, 108:05830–1 – 05830–5, 1 2012. doi:10.1103/PhysRevLett.108.058301.
15. Wojciech Samek, Grégoire Montavon, Sebastian Lapuschkin, Christopher J Anders, and Klaus-Robert Müller. Explaining deep neural networks and beyond: A review of methods and applications. *Proc. IEEE*, 109:247–278, 2021. doi:10.1109/JPROC.2021.3060483.
16. Max Veit, David M. Wilkins, Yang Yang, Jr. DiStasio, Robert A., and Michele Ceriotti. Quantum mechanical dipole moments in the QM7b, 21k molecules of QM9, and MuML showcase datasets, 6 2020. doi:10.24435/materialscloud:2k-3h.
17. Vivin Vinod, Ulrich Kleinekathöfer, and Peter Zaspel. Optimized multifidelity machine learning for quantum chemistry. *Mach. learn.: sci. technol.*, 5(1):015054, 03 2024. URL: <https://dx.doi.org/10.1088/2632-2153/ad2cef>, doi:10.1088/2632-2153/ad2cef.
18. Vivin Vinod, Sayan Maity, Peter Zaspel, and Ulrich Kleinekathöfer. Multifidelity machine learning for molecular excitation energies. *J. Chem. Theory Comput.*, 19(21):7658–7670, 2023. PMID: 37862054. doi:10.1021/acs.jctc.3c00882.
19. Vivin Vinod and Peter Zaspel. Assessing non-nested configurations of multifidelity machine learning for quantum-chemical properties. *Mach. Learn.: Sci. Technol.*, 5(4):045005, 10 2024. doi:10.1088/2632-2153/ad7f25.
20. Vivin Vinod and Peter Zaspel. QeMFi: A Multifidelity Dataset of Quantum Chemical Properties of Diverse Molecules, 2024. [arXiv:2406.14149](https://arxiv.org/abs/2406.14149).
21. Vivin Vinod and Peter Zaspel. QeMFi: A Multifidelity Dataset of Quantum Chemical Properties of Diverse Molecules [dataset], 10 2024. doi:10.5281/zenodo.13925688.
22. Julia Westermayr, Michael Gastegger, Kristof T. Schütt, and Reinhard J. Maurer. Perspective on integrating machine learning into computational chemistry and materials science. *J. of Chem. Phys.*, 154(23):230903, 06 2021. doi:10.1063/5.0047760.
23. Julia Westermayr and Philipp Marquetand. Machine learning for electronically excited states of molecules. *Chem. Rev.*, 121:9873–9926, 11 2020. doi:10.1021/acs.chemrev.0c00749.
24. Peter Zaspel, Bing Huang, Helmut Harbrecht, and O. Anatole Von Lilienfeld. Boosting quantum machine learning models with a multilevel combination technique: Pople diagrams revisited. *J. Chem. Theory Comput.*, 15(3):1546–1559, 2019. URL: <https://doi.org/doi/10.1021/acs.jctc.8b00832>, doi:10.1021/acs.jctc.8b00832.